Continual skipping on water

I. J. HEWITT[1]†, **N. J. BALMFORTH**[1] AND **J. N. McELWAINE**[2]

[1]Department of Mathematics, University of British Columbia, Vancouver, V6T 1Z2 Canada

[2]Department of Applied Mathematics and Theoretical Physics, University of Cambridge, Cambridge CB3 0WA, UK

Experiments are conducted to study the planing and skipping of a rectangular paddle on the surface of a shallow stream. The paddle is allowed to move freely up and down by attaching it to a pivoted arm. A steady planing state, in which the lift force from the water balances the weight on the paddle, is found to be stable for small stream velocities but to become unstable above a certain threshold velocity which depends upon the weight and the angle of attack. Above this threshold, the paddle oscillates in the water and can take off into a continual bouncing, or skipping, motion, with a well-defined amplitude and frequency. The transition is sometimes bistable so that both a steady planing state and a regular skipping state are possible for the same experimental parameters. Shallow-water theory is used to construct simple models that explain the qualitative features of the planing and skipping states in the experiments. It is found that a simple parameterisation of the lift force on the paddle proportional to the depth of entry is not sufficient to explain the observations, and it is concluded that the rise of water ahead of the paddle, in particular the way this varies over time, is responsible for causing the planing state to become unstable and for enabling a continual skipping state.

Key words: hydraulics, instability

---

1. Introduction

When an object impacts on a water surface, it receives an impulse that can deflect its course and may even be sufficient to cause it to rebound from the surface. This impulse is what allows us to skip stones at the beach, throwing a flat stone into the water in such a way that it bounces several times before eventually sinking. If an object is towed quickly over a water surface, on the other hand, a lift force is also generated, allowing the object to glide, or plane, along the surface, as exploited by a water skier.

In this paper we report experiments in which a rectangular plate, or *paddle*, is suspended at an angle over a fast-flowing stream and allowed to move freely up and down (see figure 1). The relative velocity of the stream and the paddle generates a lift force, and we are interested in the induced vertical motion of the paddle. Our main findings are that there are two primary dynamical states for the paddle: at low flow speeds a steady *planing* state exists, in which the lift force balances the weight

† Email address for correspondence: hewitt@math.ubc.ca

of the paddle. When the stream is sufficiently fast, on the other hand, a *skipping* state arises, in which the paddle bounces continually off the water surface without decaying. Further still, we find that the steady planing state becomes unstable, and instead the paddle will, of its own accord, 'take off' from the surface, bouncing with larger amplitude until a regular skipping state is reached. In some cases a reservoir of water builds up ahead of the paddle and a third, *sloshing*, state occurs, in which the paddle oscillates in contact with the water, and the oscillations resonate with a seiche in the reservoir upstream.

Section 2 describes the experiments and observations in more detail. In §§ 3–5, we then rationalise these observations, using simple fluid-mechanical models. Although it is perhaps intuitive that an object towed sufficiently fast will start to skip rather than plane over the surface, a simple theory to predict this is not as straightforward as one might think.

Two-dimensional models for planing have appeared previously (Green 1935, 1936; Wagner 1932; Ting & Keller 1974; Tuck & Dixon 1989; Sugimoto 2003). In these existing models the flow is assumed to be sufficiently fast so that a distinct jet is thrown well upstream without affecting the incoming flow. Such a jet is observed in our experiments when the paddle enters the fluid during skipping. In the steady planing state, however, we see that any such jet collapses rapidly to create a turbulent wedge of fluid much like that preceding the bow of a ship (Payne 1994; see figure 2).

A related body of research looks at 'water entry' problems, which have applications to the impact of torpedoes and bombs on the surface, and the forces on a seaplane's floats during landing (Wagner 1932; Mayo 1945; Johnson 1998). The main question in this case is whether the force exerted is large enough to cause ricochet off the surface (usually not desired, although famously put to effect by Barnes Wallis's 'bouncing bomb' during the Second World War). Mathematical models have been developed for the hydrodynamic response in the initial stages of an impact on both shallow and deep water (Howison, Ockendon & Wilson 1991; Korobkin 1999; Howison, Ockendon & Oliver 2004; Korobkin & Iafrati 2005); taking account of all the details of the water flow makes the results quite complicated, and these models do not easily extend so far as to allow for the object to exit the water again, as is necessary to account for skipping.

A much simpler description of the force on the entering object has been used to describe experiments on skipping stones (Clanet, Hersen & Bocquet 2004; Rosellini *et al.* 2005). In this model, which is discussed further in § 3, the lift force on the stone is essentially proportional to its distance beneath the undisturbed water surface and therefore provides a restoring force just like a linear spring. We find that such a model is too simplistic to explain our observations; in the experiment we find 'bounces' off the water surface that are superelastic, in the sense that the vertical velocity is larger coming out of the water than entering it. This cannot be explained by a conservative force, and we suggest that the missing instability mechanism is due to a 'splash-up' region that forms ahead of the paddle, as included in the more complex models mentioned above. In order to produce a theory which is simple enough to predict the trajectory of the paddle, we generalise the model used by Tuck & Dixon (1989) for flow beneath a surf skimmer. The fact that the size of the splashed-up region ahead of the paddle is not an instantaneous function of the paddle's depth (as would be the case if one simply used measured fits for the lift force on a planing object) is crucial, and we will show that allowing for this time lag is sufficient to explain why the paddle starts to skip continuously.
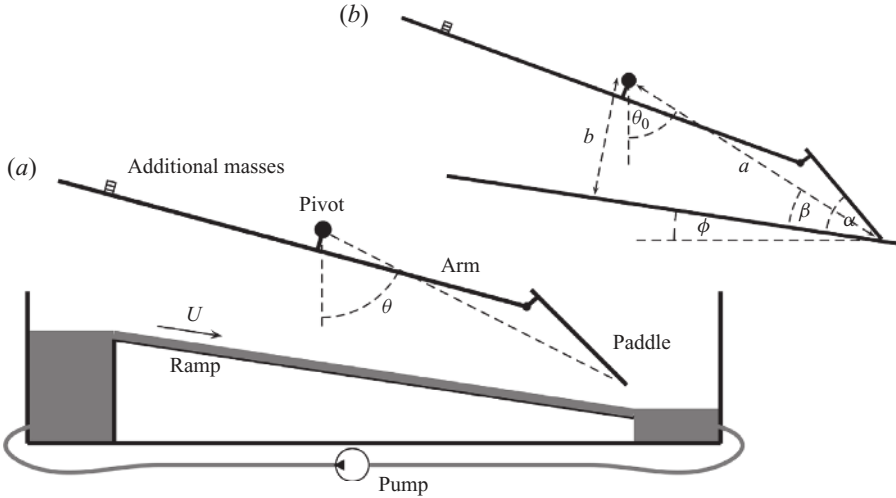
FIGURE 1. A sketch of the experimental set-up, showing the notation used in the text. (*a*) The paddle out of the water. The orientation of the paddle tip about the pivot, as measured by the sensor, is described by θ. (*b*) The paddle resting on the ramp, when $\theta = \theta_0$, and the definition of the other constant angles: the inclination of the ramp is ϕ; the angle of attack of the paddle is α; the angle between the pivot, paddle tip and ramp is β, which is related to θ_0 by $\theta_0 + \phi + \beta = \pi/2$. The distance of the paddle tip from the pivot is $a \approx 350$ mm. Masses could be added to counterbalance the paddle and alter the net moment. The total mass of the pivoted assembly is large compared with any added masses, so the moment of inertia remains roughly the same for all experiments; $\mathscr{I} \approx 0.01$ kg m^2.

2. Experiments

2.1. *Experimental set-up*

The experiments were conducted in a Perspex tank, 0.1 m wide and approximately 1 m long. A sloping ramp was inserted into the middle of the tank, dividing it into two separate reservoirs, as shown in figure 1. The upper reservoir was filled up to the level of the top of the ramp, where it overflowed and produced a shallow stream down the ramp. The water in the reservoir at the bottom was then pumped back to the top, resulting in a continual uniform flow down the ramp, with typical depths of 3–6 mm.

Above the ramp, a rectangular Plexiglas paddle was suspended by a long arm to a pivot so that it could rotate freely in the plane perpendicular to the water flow. We denote θ as the angle between the paddle tip, the pivot and the vertical (see figure 1) and θ_0 as its value when the paddle is resting on the ramp. A magnetic sensor (POSIROT from ASM Ltd, part no. PRAS1-30-U2-CW-M12 modified to operate at 2 kHz) attached to the pivot supporting the arm, measured $\theta - \theta_0$ at a sampling rate of 5 kHz, with an accuracy better than 0.01°. Because the pivot was positioned well upstream of the paddle (with $b \ll a$ in figure 1) and the angular excursions were small ($\theta - \theta_0$ was typically less than 2°), the perpendicular displacement of the paddle tip above the ramp, h_T, is related to $\theta - \theta_0$ by

$$h_T = a \cos(\theta + \phi) - a \cos(\theta_0 + \phi) \approx a(\theta - \theta_0) \cos \beta + O((\theta - \theta_0)^2), \quad (2.1)$$

where ϕ and β are defined in figure 1 and a is the distance from pivot to paddle tip.

The angle the paddle made with the ramp (whilst resting on it) is termed the 'angle of attack', α, and was varied between 24° and 88°. Two types of paddle were
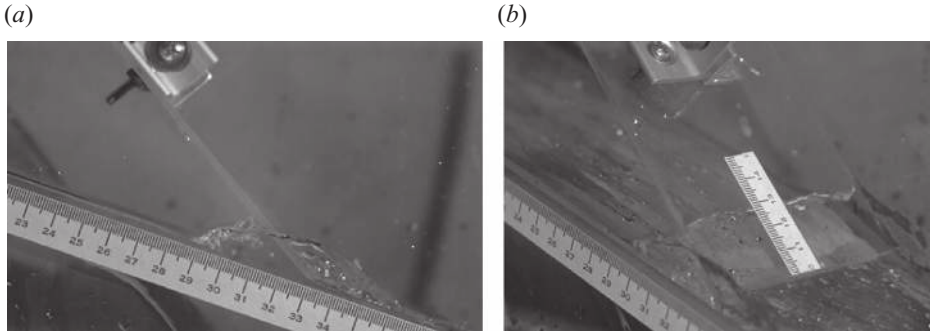
FIGURE 2. The steady planing state for the wide paddle viewed (*a*) from the side and (*b*) from slightly behind.

used: the 'wide' paddle took up almost the full width of the tank with approximately 1 mm gaps on either side, whereas the 'narrow' paddle was half the tank width and was positioned in the centre of the stream.

The weight of the paddle resulted in a moment about the pivot which caused it to fall onto the water; it could, however, be counterbalanced on the other side, to a greater or lesser extent, by adding additional masses on the arm, thereby altering the *net* moment M forcing the paddle down onto the ramp. Note that some care is needed to define the moment properly, because the rotation about the pivot of the overall centre of mass changes the component of gravity contributing a moment: if the centre of mass m is a distance l_c from the pivot and at an angle θ_c from the paddle-pivot line, the moment is $m l_c g \sin(\theta - \theta_c)$. Since the paddle's orientation varies by only a small amount (i.e. $\theta - \theta_0 \ll \theta_0 - \theta_c$), this change is for the most part small compared with the moment itself. For very small moments, however, the change becomes more significant, and when the paddle is very close to being counterbalanced, the system starts to behave like a pendulum, with the moment even changing sign as the paddle moves back and forth about its equilibrium orientation. We therefore define M to be the moment the paddle experiences when it is resting on the ramp. Negative moments in the data (see, for example, figure 5) are due to the fact that the paddle's equilibrium position was slightly above the level of the ramp but below the water surface.

We also varied the stream velocity by changing the inclination of the ramp. The velocity was measured by tracking particles in high-speed video footage of the flow, with an accuracy of approximately $\pm 0.05 \, \mathrm{m \, s^{-1}}$; varying the ramp angle ϕ between $2°$ and $16°$ caused the velocity to vary between approximately 0.6 and $1.2 \, \mathrm{m \, s^{-1}}$. Experimental runs typically involved a fixed choice of stream velocity and angle of attack, whilst the extra mass added to the arm was treated as the main control parameter.

Before describing the results of the experiments, it is worth estimating the importance of various physical effects: given that $U \sim 1 \, \mathrm{m \, s^{-1}}$ and $H \sim 5 \, \mathrm{mm}$, the Reynolds, Froude and Weber numbers are estimated as

$$Re = \frac{UH}{\nu_w} \approx 5000, \qquad Fr = \frac{U}{\sqrt{gH}} \approx 5, \qquad We = \frac{\rho U^2 H}{\sigma} \approx 100, \qquad (2.2)$$

in which g is the gravitational acceleration, ρ is the density of water, ν_w is the kinematic viscosity, and σ is the surface tension. Within the bulk of the stream, the predominant hydrodynamic forces are therefore expected to be inertial; capillary effects are almost certainly negligible, and gravitational effects are small over distances
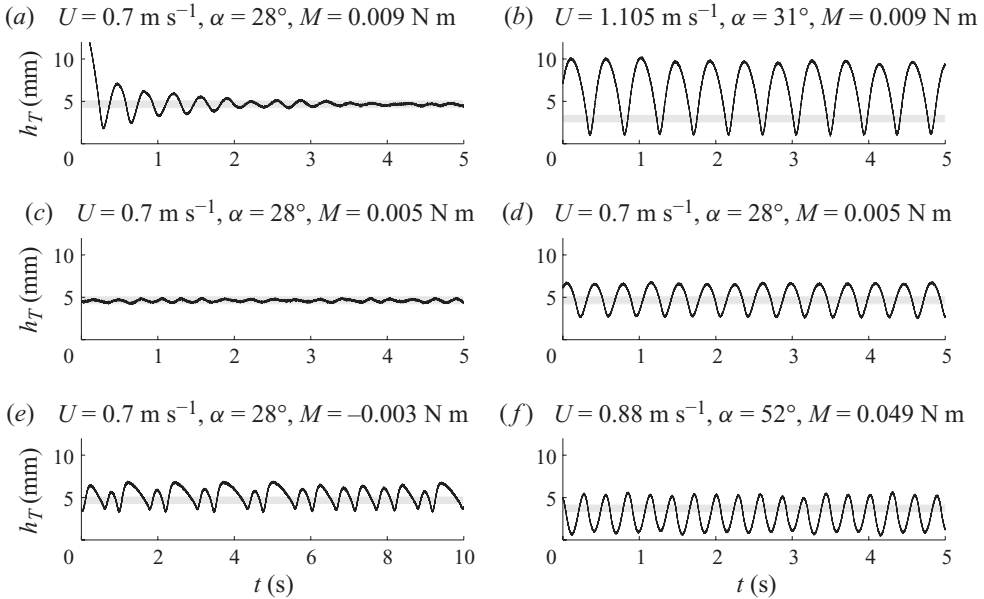
(a) $U = 0.7 \text{ m s}^{-1}$, $\alpha = 28°$, $M = 0.009 \text{ N m}$ (b) $U = 1.105 \text{ m s}^{-1}$, $\alpha = 31°$, $M = 0.009 \text{ N m}$

(c) $U = 0.7 \text{ m s}^{-1}$, $\alpha = 28°$, $M = 0.005 \text{ N m}$ (d) $U = 0.7 \text{ m s}^{-1}$, $\alpha = 28°$, $M = 0.005 \text{ N m}$

(e) $U = 0.7 \text{ m s}^{-1}$, $\alpha = 28°$, $M = -0.003 \text{ N m}$ (f) $U = 0.88 \text{ m s}^{-1}$, $\alpha = 52°$, $M = 0.049 \text{ N m}$

FIGURE 3. Sample trajectories from the experiments with a wide paddle; the grey band shows the position of the undisturbed water surface. (a) A steady planing state, when the paddle is dropped from just above the surface. (b) A skipping state with similar angle of attack and moment as (a), but with much faster water velocity. (c, d) A bistable situation with both a steady planing state and a persistent oscillating state. (e) An irregular state, when the paddle is very close to being counterbalanced. (f) A sloshing state, when the angle of attack and moment are somewhat larger.

of the order of the flow depth. This is not to say that gravity and surface tension do not play a role: gravity is important in bringing any splashed-up water back down into the stream, and surface tension visibly played a role in the dynamics of detached droplets.

2.2. *Observations*

As described more fully below, varying the applied moment M reveals two main types of dynamical behaviour for the paddle, planing and skipping, along with a distinctive transition between the two; in addition, sloshing states could also be observed for the wide paddle. Sample trajectories of the height of the paddle tip, h_T, illustrating the different types of behaviour are shown in figure 3. 'Regime diagrams' are presented in figure 4 and indicate the areas on either the (M, U) or the (M, α) parameter plane where the various states were observed.

From time series such as those shown in figure 3 we extract the mean height of the paddle tip, the average peak-to-trough amplitude A and the average frequency of oscillation f (from the mean peak-to-peak time interval) to provide quantitative measures of the dynamics. The mean paddle depth furnishes a key measurement for the planing states, whereas A and f characterise the skipping oscillations. A typical pattern for how the amplitude and frequency vary with moment is shown in figure 5 and clearly exposes the transition from planing at larger M to skipping at small M. Note that the error bars in A represent the standard deviation of all the peak-to-trough amplitudes measured in each time series; the size of these error bars therefore characterises the regularity of the skipping oscillations.
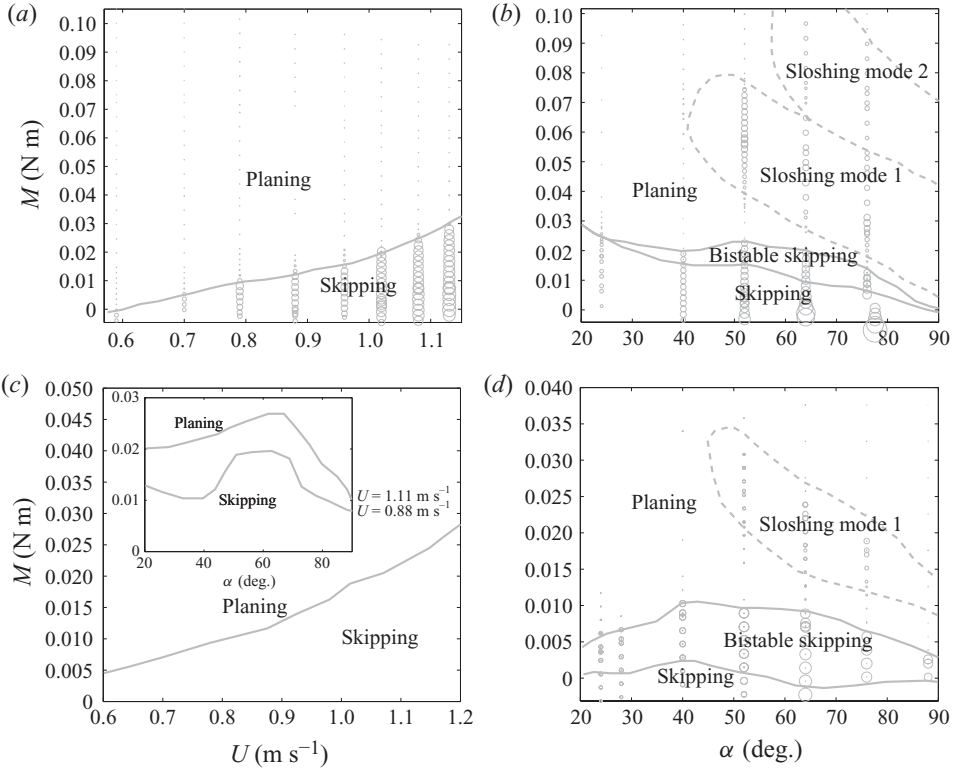
FIGURE 4. Regime diagrams for planing, skipping and sloshing. (*a*) Sketch of the different regimes for the wide paddle with an angle of attack $\alpha = 36°$ and varying velocity U and moment M. The size of each circle represents the amplitude of variations in h_T, and the regime boundaries have been further constrained by additional experimental runs with intermediate values of the parameters for which detailed measurements were not made. (*b*, *d*) Similar sketches for $U = 0.88$ and $0.7\,\mathrm{m\,s^{-1}}$, respectively, with varying angles of attack α and moment M. In (*c*), for the narrow paddle, the approximate transition from planing to skipping is shown for angle of attack $\alpha = 40°$. The inset shows the dependence on the angle of attack for two values of U.
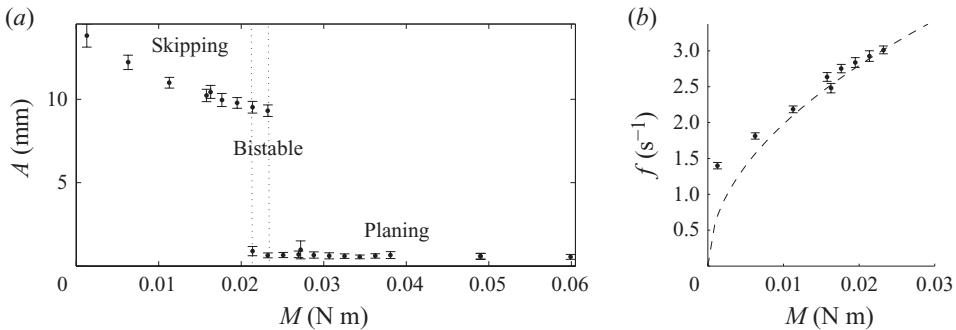

FIGURE 5. (*a*) Mean amplitudes (average peak-to-trough change in h_T) for varying moments for the wide paddle, with velocity $U = 1.11\,\mathrm{m\,s^{-1}}$ and angle of attack $\alpha = 40°$. For each data point, the error bars show the standard deviation incurred within each time series; the fact that these are small indicates that the bounces are relatively regular. (*b*) Corresponding frequency of skipping states. The error bars show the standard deviation. The dashed line shows $f = (Ma\cos\beta/8\mathscr{I}A)^{1/2}$ for $A = 10\,\mathrm{mm}$ (see § 2.4).
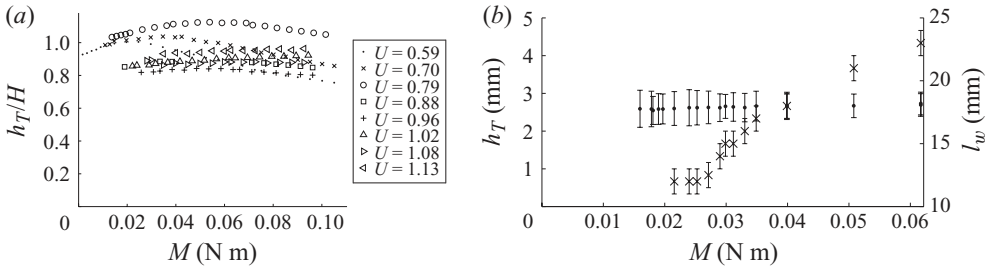
FIGURE 6. (*a*) Heights of the paddle tip, scaled with the water depth, during steady planing states for the wide paddle, for varying moment, $\alpha = 36°$ and several different water velocities as indicated. (*b*) Heights of the wide paddle during steady planing states (left axis, dots) and the corresponding wetted length on the paddle (right axis, crosses) for velocity $U = 1.11\,\mathrm{m\,s}^{-1}$ and angle of attack $\alpha = 49°$.
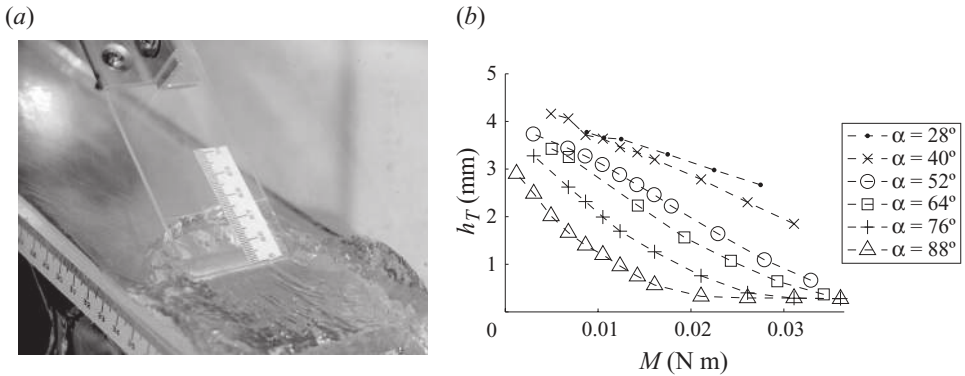

FIGURE 7. (*a*) The steady planing state for the narrow paddle. (*b*) Heights of the paddle tip are shown for varying moment, $U = 0.7\,\mathrm{m\,s}^{-1}$ and different angles of attack as indicated.

2.3. *Planing states*

When the moment is large enough, the paddle fluctuates at a low level about a steady height, due to vagaries of the flow rate and stream depth. Lifting the paddle up and dropping it into the stream results in damped oscillations back to the steady planing height as seen in figure 3(*a*).

Figure 2 shows photographs of a sample steady planing state for the wide paddle; there is a turbulent 'wedge' of water that builds up ahead of the paddle, with very little loss of water around the sides. Somewhat surprisingly, and as illustrated in figure 6(*a*), the height of the paddle tip appears to be almost the same as the undisturbed water depth, H, and does not show any significant increase with the moment. The greater moment must be supported by a larger force from the water, but this does not result from deeper penetration into the stream; instead, it results from a larger wedge being built up ahead of the paddle, as indicated by the increase of the wetted length shown in figure 6(*b*).

The narrow paddle also builds up a turbulent wedge, although a significant fraction of the water is now diverted around the sides (figure 7). Steady depths of the narrow paddle for several different angles of attack are shown in figure 7. All the data show a definite decreasing trend with increasing moment, in contrast to the case for the wide paddle. At the same time, the wetted length of the paddle increases, as for the wide paddle. At the highest moments, the flow becomes completely diverted around
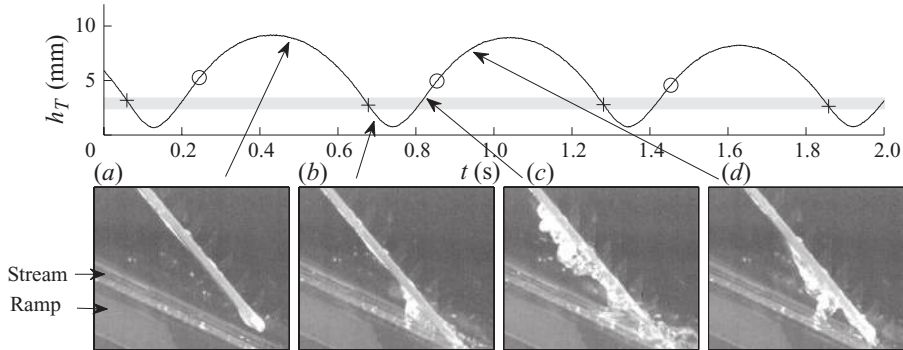
FIGURE 8. A trajectory of the height of the tip of the narrow paddle showing times of entry (pluses) and exit (circles), as determined from high-speed video footage of the bounce. Example images during the cycle show the paddle (*a*) near the top of its airborne trajectory, (*b*) shortly after entering the water, when the jet can be seen spreading up its front, (*c*) as it leaves the water, with a large jet of water still attached, and (*d*) above the water surface, as the jet falls back into the stream. The stream is seen as the relatively narrow band of grey, above a much wider grey band which is the ramp.

the sides, and the paddle rests on the bottom of the stream, leading to the levelling out of the data for the highest angles of attack in figure 7 (the fact that this appears to be just above the bottom is due to an error of ± 2.5 mm in measuring the origin for h_T).

2.4. *Skipping states*

For smaller net moments, the paddle exhibits a constant skipping mode, characterised by a relatively regular oscillation, an example of which is seen in figure 3(*b*). For very small moments, the majority of the motion is out of the water, following a ballistic trajectory in the air and 'bouncing' off the water surface very much like an elastic ball.

Skipping behaviour occurs in much the same way for both the wide and the narrow paddle, and an example for the narrow paddle is shown in figure 8. When the paddle enters the water a thin high-speed jet is ejected up the front, rising several centimetres. This jet remains in contact with the paddle even until after it has been pushed back out of the stream. By analysing video footage of the motion, both from the side and from behind the paddle, it was possible to distinguish between the jet and the bulk of the stream and therefore to determine the moments at which the paddle enters and leaves the stream, as shown in figure 8. Some time later, the jet detaches from the paddle and falls back into the stream.

It is evident from figure 8 that the paddle exits the stream at a much higher position than at which it entered. Simultaneous video footage reveals that whilst the paddle is entering the water, the stream builds up a wedge ahead of it (in addition to the thin jet ejected from the top of the wedge); as the paddle is forced back up again, it remains in contact with the water until it clears the top of the wedge. This, we believe, is fundamental in allowing the paddle to skip continually; the build-up of the wedge essentially means that the paddle is in contact with the water for longer on the way out than on the way in, allowing it to be accelerated to a larger speed than that with which it entered.

The skipping amplitude selects itself; the paddle can be dropped from any height above the water, and the subsequent oscillations will evolve to the same average amplitude. If the initial amplitude is smaller, successive oscillations grow, showing
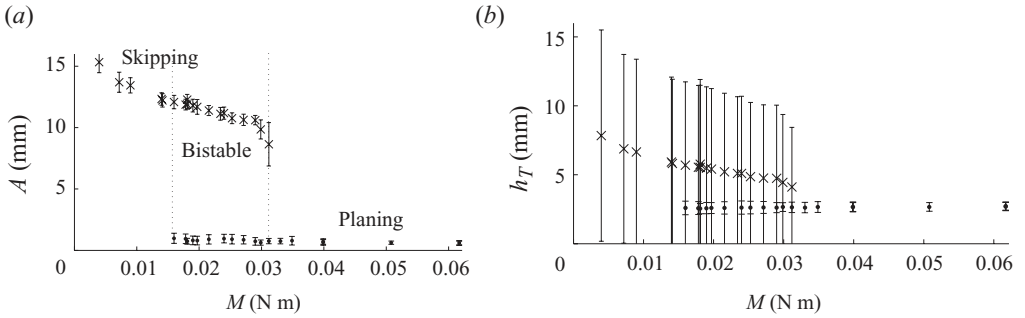
FIGURE 9. (*a*) Mean oscillation amplitudes *A* for the wide paddle for varying moment, with velocity $U = 1.11\,\mathrm{m\,s^{-1}}$ and angle of attack $\alpha = 49°$. The dots show steady planing states; the crosses show regular skipping states (the error bars show the standard deviation of amplitude of oscillations). (*b*) Mean height of paddle above the ramp for the same experiments. The error bars here show the range of h_T.

that low-amplitude bounces off the water surface are *superelastic*. The mean amplitude depends upon the moment, as is seen in figure 5, generally decreasing as *M* increases. For smaller-amplitude skipping states, it is very hard to tell whether the paddle leaves the water during the motion or not, since the water surface beneath the paddle is severely disturbed. There do appear to be some cases, however, in which the paddle does not leave the water surface. For large angles of attack, and for large amplitude skips, the paddle touches the ramp at the bottom of the stream, and the bounce arises from a combination of that impact and the force from the water. For shallower angles, however, the paddle always remains above the bottom of the stream.

Note that the skipping frequency shows a definite decreasing trend with decreasing moment (see figure 5*b*). This is largely the result of the decrease in the effective acceleration of the paddle during its ballistic trajectory above the water (the moment of inertia of the arrangement being largely unaffected by the weights added to the arm). Indeed if the paddle were bouncing elastically on the ramp and following a perfectly ballistic trajectory, the frequency would vary as $f \propto M^{1/2}$, as illustrated by the dashed line in figure 5(*b*). (As seen in the next section the equation of motion in that case is $\mathcal{I}\ddot{\theta} = -M$; the trajectories are $\theta - \theta_0 \approx A/a \cos\beta - Mt^2/2\mathcal{I}$, given that an amplitude *A* corresponds to $\theta - \theta_0 \approx A/a \cos\beta$, and the time between bounces is $(8\mathcal{I}A/Ma\cos\beta)^{1/2}$.) The frequency data for the skipping paddle do not quite follow this trend because the moment varies with height, and the paddle spends some time in the water.

2.5. *Transition between planing and skipping*

For a fixed stream velocity and angle of attack, the skipping state typically ceases abruptly above a threshold moment, as seen in figure 5. The paddle then rests in its steady planing state as discussed above. It can be lifted and dropped into the stream to try and excite it into the skipping state, but will slowly decay back to the planing state.

This threshold for the regular skipping state does not necessarily correspond to the loss of stability of the planing state, however. As is clear from figure 5 there can be a range of moments for which the paddle is bistable, being able to exist in either a regular skipping state *or* a steady planing state. This is also shown in figure 9, where there is a larger range of moments for which there are two possible states. One can select between the two states by either lifting the paddle and dropping it from
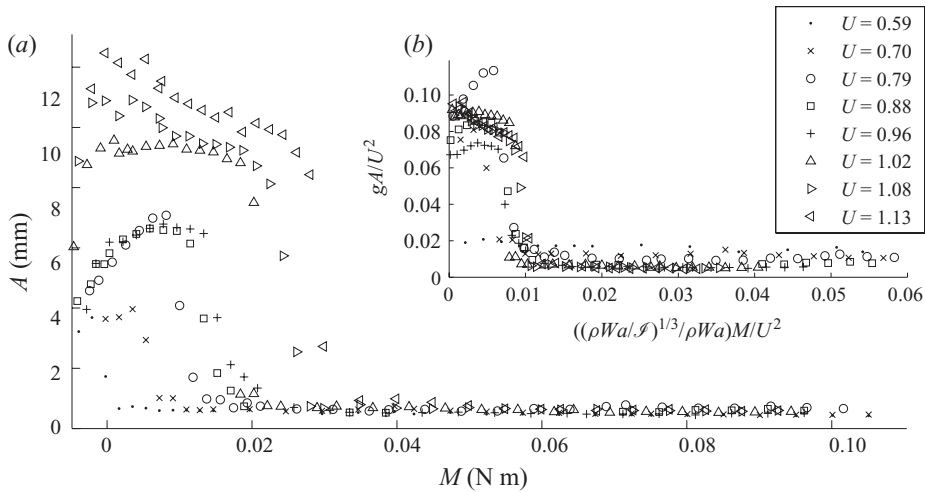
FIGURE 10. (*a*) Mean amplitudes A for the wide paddle for varying moments and for eight different velocities, all with angle of attack $\alpha = 36°$. (*b*) The inset shows the same data, dimensionlessly plotted using the quantities gA/U^2 and $(\rho Wa/\mathcal{I})^{1/3}M/\rho WaU^2$, showing a collapse of the bifurcation threshold.

above or placing it gently in the water. The system will very occasionally exhibit a spontaneous transition from skipping to planing, or vice versa (because of noise); for the most part however, the two states are very robust. Figures 3(*b*) and 3(*c*) show time traces of the coexisting planing and oscillating states in one experiment.

There were some choices of the velocity and the angle of attack for which the bistable regime was not detected, and there appeared to be a smoother transition between planing and skipping (see figure 10). Generally speaking, the largest bistable regions appeared for angles of attack in the range 40°–70°, and for smaller, or larger, angles there was little or no bistability. Bistability was also much more common for the wide paddle; in fact it was observed with the narrow paddle only at the lowest stream velocities, and for faster velocities there was a smoother transition between the two states. Indeed, it was much harder to identify a well-defined threshold for skipping in these cases.

For the wide paddle, however, the threshold causes a well-defined bifurcation in the amplitude data, such as in figures 5 and 9. Figure 10 shows amplitude data for several different stream velocities, in an attempt to show how the threshold moment depends upon water speed. There is no bistability evident in these cases. As one might perhaps expect, the skipping state is possible for a larger moment (a heavier paddle) when the stream is faster. Therefore, if one could gradually increase the flow speed, for a fixed moment, there would be steady planing until a critical velocity is reached, above which it would 'take off' and start skipping continually. The rescaling of the data in figure 10(*b*) suggests that the threshold moment for instability scales with the square of the velocity.

There was a much less clear trend in the way the onset of skipping depended on the angle of attack or the width of the paddle. For larger flow speed, there was some evidence that the threshold moment decreased with the angle of attack (figure 4*b*). However, this was not always the case (see figures 4*c* and 4*d*). Overall, the dependence on the angle of attack and the paddle width seems relatively weak.
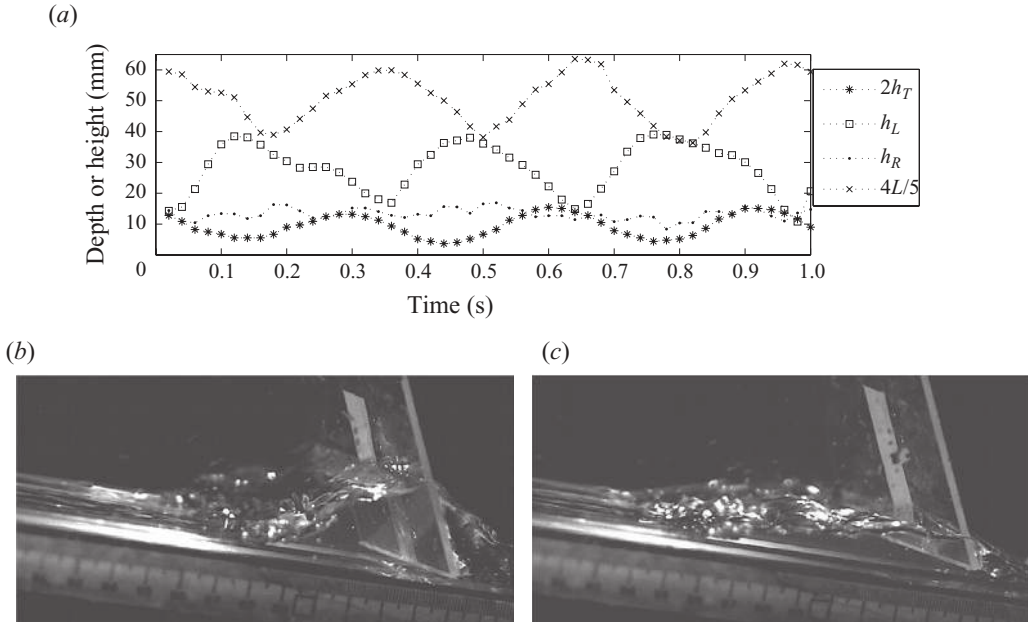
(*a*)

(*b*)

(*c*)

FIGURE 11. (*a*) Mode 1 sloshing showing the following: h_L, the depth at the leading edge of the paddle; h_T, the depth at the paddle tip; h_R, the depth roughly halfway along the reservoir; and L, the approximate length of the reservoir. These traces are obtained from analysing video footage. Example images of the sloshing wedge are shown in (*b*) and (*c*); these pictures are roughly half a period apart, with the paddle tip near its lowest height in the first image and near its highest height in the second one.

2.6. *Sloshing states*

For large angles of attack, $\alpha > 40°$, a separate unstable regime of sloshing was encountered for the wide paddle, examples of which are illustrated in figures 3(*f*), 11 and 12. Sloshing occurred at larger moments than skipping, when the force to balance the moment required a large wedge-shaped reservoir to be built up in front of the paddle. The sloshing corresponded to a regular oscillation of the paddle that was tuned to coincide with the rocking back and forth of the water in the reservoir (i.e. a seiche). As indicated in figures 11 and 12, two different modes of sloshing were observed, corresponding to different flow patterns in the reservoirs (i.e. seiche modes): in the first (termed mode 1 in figure 4 and pictured in figure 11), the motion at either end of the reservoir is out of phase (moving up at one end and down at the other), whilst in the second (mode 2 in figure 4 and pictured in figure 12), the ends are in phase (moving up at both ends simultaneously).

When sloshing occurred, the steady planing state appeared to be unstable: the 'bifurcation diagrams' of figure 13, displaying paddle amplitude A and frequency f against moment M, show no evidence for bistability or abrupt changes in amplitude, except over the transition from planing to skipping at lower moment. The second pair of these diagrams (figures 13*b* and 13*d*) also clearly distinguishes the two different sloshing modes, which emerge for different, but adjacent, ranges of moment. The frequency of each sloshing mode generally decreases with increasing moment, in contrast to the skipping states (see figure 13). This trend may be associated with a
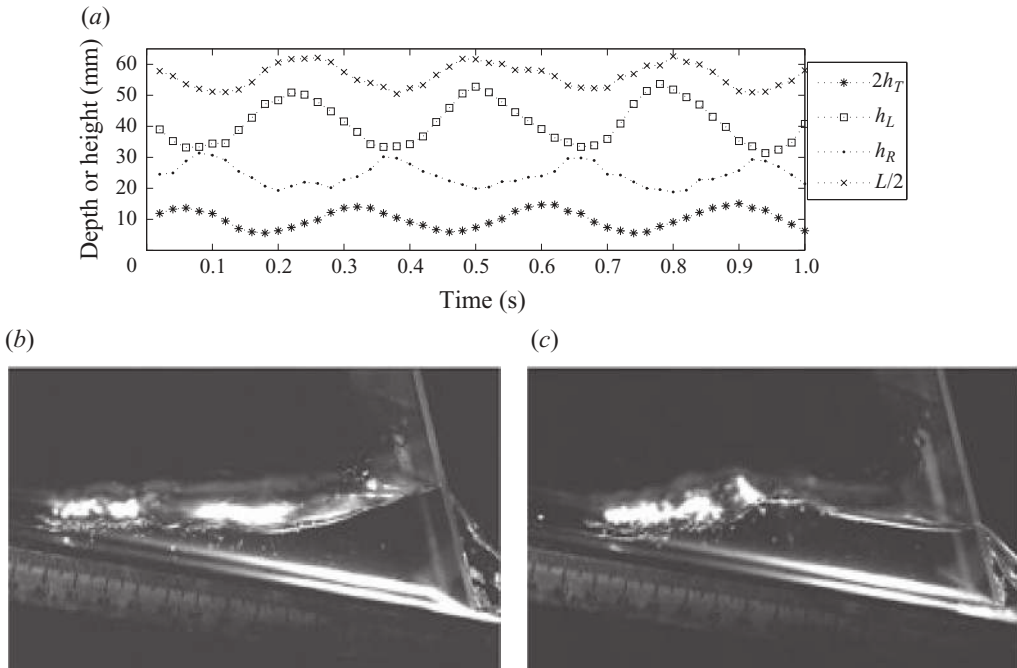
(a)

(b)

(c)

FIGURE 12. (a) Mode 2 sloshing showing a similar plot as figure 11 with the same notation. Note that in this case the reservoir is much longer, and h_L and L are in phase, contrary to the mode 1 case in figure 11. Example images of the sloshing reservoir are shown in (b) and (c); these pictures are roughly half a period apart, with the paddle tip near its lowest height in the first image and near its highest height in the second one.
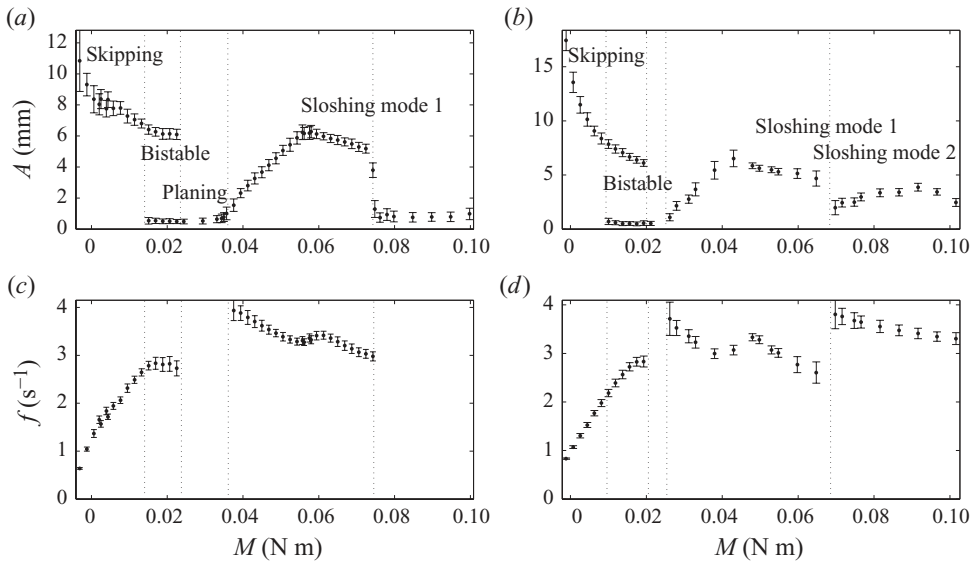
(a)

(b)

(c)

(d)

FIGURE 13. (a) Mean amplitudes A for the wide paddle for varying moment, with $U = 0.88\,\mathrm{m\,s^{-1}}$ and $\alpha = 52°$, showing distinct skipping, planing and sloshing regimes. The error bars show the standard deviation. (b) A similar plot of the amplitude of oscillations for $U = 0.88\,\mathrm{m\,s^{-1}}$ and $\alpha = 64°$, in which there are two separate peaks to the sloshing regimes. (c, d) The frequency of oscillations for the sloshing and skipping cases shown in (a) and (b).

decrease in the natural frequency of seiche modes, since the reservoir length must increase to balance larger moments.

3. Preliminary theoretical framework

Before building models for the planing and skipping states, we first outline some preliminary theoretical ideas. In part we pave the way for the later models. However, we also take this opportunity to demonstrate that overly simple models of the fluid dynamics are not sufficient to reproduce the experimental phenomenology.

As mentioned in the Introduction, the dynamics are similar to those that occur for a skipping stone or a surf skimmer, and previous models of those situations serve as a useful starting point. Our experiment is of course not exactly the same, since the paddle is constrained to move in an arc, and the presence of the channel walls and the rectangular shape of the paddle are further obvious differences. Nevertheless, the paddle's motion out of the water is predominantly normal to the stream, and when exhibiting discrete bounces the dynamics appears very similar to a skipping stone, but with the horizontal velocity held fixed. Surf skimming (Tuck & Dixon 1989) involves a surfboard planing on a shallow-water layer and generating lift.

3.1. *Equation of motion of the paddle*

Since the Reynolds number is large, viscous forces can be ignored, so we take the force on the paddle to be entirely normal to its surface and due to the pressure of the water in contact. The pressure has both dynamic and hydrostatic components, but we ignore the latter, since dynamic pressures are $O(Fr^2)$ larger. This is a reasonable approximation for many of the experiments, but is less suitable for the larger moments when the stream depth ahead of the paddle builds up and the hydrostatic component becomes more important.

Since the wetted length of the paddle is very small compared with the arm length a, the normal force F_n can be treated as acting at the end of the paddle tip, and it therefore exerts a moment $F_n a \cos(\alpha - \beta)$, which opposes the net moment due to the effective weight. As discussed previously, the latter moment depends slightly upon the angle of the arm, but we ignore this effect here and treat M as constant. The equation of motion for the arm is therefore

$$\mathscr{I}\ddot{\theta} = F_n a \cos(\alpha - \beta) - M, \qquad (3.1)$$

where $\mathscr{I}$ is the moment of inertia of the whole pivoted system. We use (2.1) to convert this to an equation for the paddle tip's displacement d below the initial water surface, related to its height h_T and the stream depth H by

$$d = H - h_T \approx H - a(\theta - \theta_0)\cos\beta. \qquad (3.2)$$

The equation of motion can therefore be written as

$$I\ddot{d} = M - F_n a \cos(\alpha - \beta) - \nu\dot{d}, \qquad (3.3)$$

in which we define the constant $I = \mathscr{I}/a\cos\beta$ to represent inertia. In (3.3) we have also added an additional damping term with the simple form $-\nu\dot{d}$, which can, in principle, account for any air resistance to the paddle or friction in the hinge. However, fits of solutions to (3.3) with $F_n = 0$ to the ballistic trajectories recorded in the experiments (with or without water flow down the ramp) suggest that such sources of dissipation are largely insignificant. More important is the dissipation incurred when the paddle

enters the water because of effects such as turbulent drag. Unfortunately the form of such a drag in (3.3) is not particularly clear and depends on the how deep the paddle is in the water, varying in a complicated way throughout the oscillations. Instead, we retain $-\nu\dot{d}$ as a crude parameterisation that allows us to gauge the general effect of dissipation on the dynamics of the arm. The appropriate value of ν probably depends upon parameters such as U and α, and therefore differs from experiment to experiment.

3.2. *Previous planing models*

A number of mathematical models for the steady planing of a paddle in the absence of gravity have been put forward in the past and provide a convenient expression for F_n. Wagner (1932) studied the case of infinitely deep water, and Green (1935) studied the equivalent problem on a finite depth stream; Green found that the normal force on a paddle can be written:

$$F_n = \cot(\alpha/2)\rho W U^2 d, \qquad (3.4)$$

where $\rho = 1000\,\mathrm{kg\,m^{-3}}$ is the water density, W is the paddle's width, U is the stream velocity, and d is the displacement of the trailing edge beneath the undisturbed surface level. Essentially the same result, that the force depends linearly on the depth of the trailing edge, was found by Tuck & Dixon (1989). A common feature of all of these models is a splash jet ejected ahead of the leading edge.

Ejected jets are not, however, found in the steady planing state in our experiments (figure 2), because gravity acts to pull the jet back down into the stream. One might expect that there could be a steady situation in which the jet follows a ballistic trajectory ahead of the leading edge and lands on the surface some distance upstream, recirculating some of the incoming water. An asymptotic analysis of such a flow geometry on infinitely deep water was considered by Ting & Keller (1974). There was some evidence for this type of jet when the stream velocities were higher than in the experiments reported in §2. In those reported, however, in common with other experiments on planing hulls (Payne 1994), the recirculating jet collapsed and evolved into a foaming wedge such as is seen in figure 2. Thus, a normal force of the form (3.4) seems inappropriate, and we present a more obviously relevant, if crude, alternative in §4.

3.3. *Previous skipping models*

A similar normal force to (3.4) was used with apparent success to explain skipping stones (Bocquet 2003; Clanet *et al.* 2004; Rosellini *et al.* 2005). This normal force depends on the relative velocity of the paddle with respect to the water, and the area of water which it is displacing (von Kármán 1929). In our experiment the relative velocity is $\boldsymbol{U} \approx (U, -\dot{d})$ in coordinates aligned parallel and perpendicular to the stream, and the direction of motion of the paddle makes an angle $\gamma = \tan^{-1}\dot{d}/U$ with the water surface (see figure 14a). The area being displaced in the plane perpendicular to that velocity is $Wd\sin(\alpha + \gamma)/\sin\alpha = Wd(U + \cot\alpha\,\dot{d})/(U^2 + \dot{d}^2)^{1/2}$, assuming there is no build-up of water ahead of the paddle. The force can then be expressed as (Rosellini *et al.* 2005)

$$F_n = \tfrac{1}{2}\rho W(U^2 + \dot{d}^2)^{1/2}(U + \cot\alpha\,\dot{d})d. \qquad (3.5)$$

In the experiments the horizontal velocity U is much larger than the vertical velocity $\dot{d}$ ($U \approx 1\,\mathrm{m\,s^{-1}}$ and $\dot{d} \approx 0.1\,\mathrm{m\,s^{-1}}$), so we discard $\dot{d}^2$ in comparison with U^2 in (3.5) to
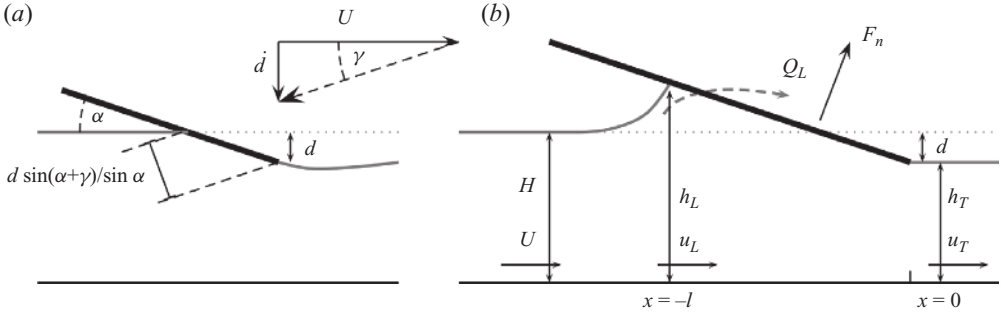
FIGURE 14. (a) Geometry of the entering paddle if the rise of water and the ejected jet ahead of the paddle are neglected, as assumed in the derivation of the force in (3.5). The relative velocity of the paddle and the stream is shown by the dashed arrow. (b) Geometry of the shallow-water model for steady planing. The water rises ahead of the paddle to produce a turbulent wedge which is in contact with the paddle in the region $-l < x < 0$. The sink Q_L accounts for flow of water around the sides of the paddle. The wetted region in this model is larger than that expected on the basis of the level of the undisturbed surface as seen in (a).
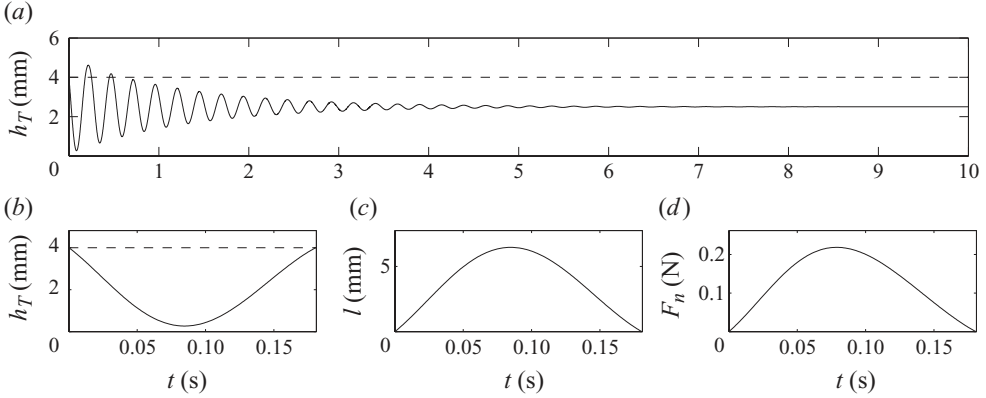

FIGURE 15. (a) Trajectory of paddle according to the skipping stone model (3.6) of Rosellini et al. (2005); (b) the paddle tip position; (c) the wetted length; and (d) the normal force, during the first bounce. The parameters are $H = 4$ mm, $U = 1.1$ m s^{-1}, $\alpha = 30°$, $M = 0.03$ N m, $I = 0.03$ kg m, $\beta = 20°$, $a = 0.35$ m and $\nu = 0$, and the initial vertical entry velocity is 50 mm s^{-1} (i.e. $d = 0$, $\dot{d} = 50$ mm s^{-1} at $t = 0$).

arrive at the equation of motion

$$I\ddot{d} = M - \tfrac{1}{2}a\cos(\alpha - \beta)\rho W U^2 d - \tfrac{1}{2}a\cos(\alpha - \beta)\rho W \cot\alpha\, U d\dot{d} - \nu\dot{d}. \qquad (3.6)$$

The last two terms are small but are important in that they add damping to a system that would otherwise be a simple harmonic oscillator. Equation (3.6) is valid whilst the paddle is in the water (i.e. when $d > 0$, in this set-up); when it is out of the water, $F_n = 0$.

The nonlinear damping term indicates that skipping motion must gradually decay; for a skipping stone, the horizontal velocity also decreases, and the stone eventually stops skipping and sinks (assuming it is not buoyant). In the current situation of sustained horizontal velocity, (3.6) indicates that the paddle tends to a steady planing state. A solution to (3.6) is shown in figure 15, in which only two small skips are produced. This model is clearly unable to explain continual skipping as observed in

the experiments. In order to explain this there must be a destabilising process, which is missing from the description of the force in (3.5).

4. A model for the steady planing states

High-speed video recordings of the turbulent wedge ahead of the paddle reveal a complicated flow structure. Rather than attempt to model the details of this flow, we instead opt for a simpler description that seeks to capture the main features of the observed planing state and, in particular, the dependence of the steady planing depth and wetted length upon the moment. Our model is based on the shallow-water set-up shown in figure 14(b), which applies for shallow angles of attack when the flow under the paddle has a small aspect ratio, and only qualitatively when paddle angles are higher. In this geometry, the paddle tip is located at $x = 0$, and the displacement beneath the undisturbed water surface H is again denoted $d = H - h_T$. The paddle's height is given for $x < 0$ by

$$h(x) = H - d - sx, \tag{4.1}$$

where $s = \tan \alpha$. The wetted region of the paddle is $-l < x < 0$ so that $x = -l$ denotes the position of the top of the turbulent wedge, where the water depth is

$$h_L = H - d + sl. \tag{4.2}$$

4.1. Wide paddle

For the wide paddle almost all the water has to flow underneath the paddle, and the situation is very close to being two-dimensional, as in figure 14. Mass conservation then requires the flux everywhere to be constant:

$$hu = HU, \tag{4.3}$$

where h and u are the stream depth and the velocity and H and U are their prescribed upstream values.

Without resolving details of the flow in the wedge region just ahead of $x = -l$, we know that the bottom of the stream, on the ramp, must be a streamline, and we use Bernoulli's principle to argue that

$$p + \tfrac{1}{2}\rho u^2 = \tfrac{1}{2}\rho U^2 \tag{4.4}$$

is a constant, which is determined from the flow far upstream where the pressure is zero (at large Froude number). Since p must also be zero at the trailing edge, this implies $u_T = U$, and therefore $h_T = H$; i.e. the paddle should rest exactly at the undisturbed water level. The pressure beneath the wetted region of the paddle is then

$$p = \frac{1}{2}\rho U^2 \left(1 - \frac{h_T^2}{h^2} \right), \tag{4.5}$$

and since $h = h_T - sx$, the normal force is given by

$$F_n = \int_{-l}^{0} pW \, \mathrm{d}x = \frac{1}{2}\rho W U^2 \frac{(h_L - h_T)^2}{s h_L} = \frac{1}{2}\rho W U^2 \frac{sl^2}{h_T + sl}. \tag{4.6}$$

For the paddle to be in a steady position, this force must balance the moment, $M = a \cos(\alpha - \beta)F_n$, and therefore

$$\frac{l^2 \tan \alpha}{H + l \tan \alpha} = \frac{2M}{a\rho W U^2 \cos(\alpha - \beta)}. \tag{4.7}$$
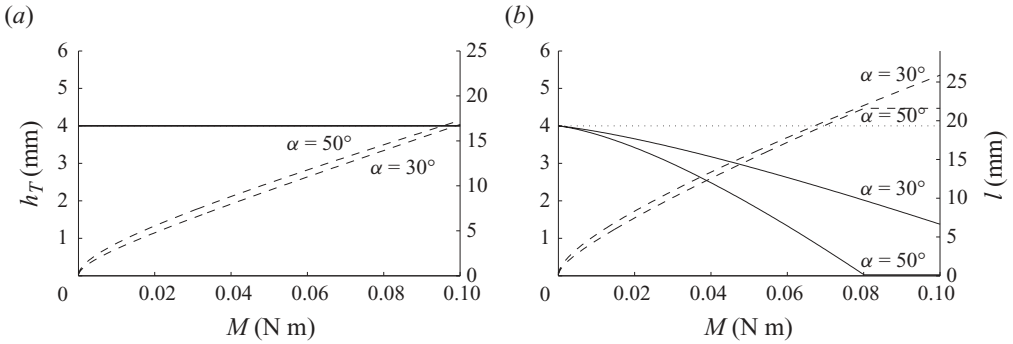
(*a*)   (*b*)

FIGURE 16. Steady-state depth (left axis, solid line) and horizontal wetted length *l* (right axis, dashed line) for two different angles of attack $\alpha = 30°$ and $\alpha = 50°$, for (*a*) the wide paddle model (4.7) and (*b*) the narrow paddle model (4.11) with $\lambda = 1$. The water depth is $H = 4$ mm, and when the paddle tip reaches the bottom of the stream, the reaction of the ramp holds the paddle in place.

Thus, for the wide paddle, we expect the steady depth h_T to be independent of the moment and equal to the undisturbed water depth H, but we expect the wetted length, and therefore the size of the wedge, to increase in order to balance larger moments. An example is shown in figure 16(*a*) and agrees qualitatively with the experimental observations displayed in figure 6.

4.2. *Narrow paddle*

The steady planing states are qualitatively different for the narrow paddle because much of the flow is diverted around the sides so that the situation is no longer two-dimensional. We incorporate this situation within the same framework by adding the flux Q_L diverted around the sides of the paddle. If we assume that this flux is lost from within the turbulent wedge just ahead of $x = -l$, then the model above still holds provided we modify (4.3) to

$$Whu = WHU - Q_L. \tag{4.8}$$

The formulae for the pressure in (4.5) and for the force in (4.6) still apply, but with $h_T = H - d$, where d is related to the diverted flow by

$$d = \frac{Q_L}{WU}. \tag{4.9}$$

It remains to determine Q_L. We expect intuitively that the amount of flow around the sides depends upon the size of the built-up wedge; the larger the wedge, the more the diverted flow. Thus (4.9) should relate the depth d to the wetted length l in a monotonic way, and the force given by (4.6) is therefore an increasing function of d or, equivalently, l.

A simple parameterisation is to take the diverted flux to be proportional to the water speed U and the cross-sectional area of the wedge (facing out of the paper in figure 14):

$$Q_L = \lambda \frac{1}{2s}(h_L - H)^2 U, \tag{4.10}$$

FIGURE 17. A sketch of the paddle and free surface during a collision.

where the constant of proportionality is a further model parameter. The steady state in this case has

$$l = \frac{d^{1/2}\left(d^{1/2} + \mu^{1/2}\right)}{\tan\alpha}, \qquad \frac{d\left(d^{1/2} + \mu^{1/2}\right)^2}{\left(H + \mu^{1/2}d^{1/2}\right)\tan\alpha} = \frac{2M}{a\cos(\alpha - \beta)\rho W U^2}, \qquad (4.11)$$

with $\mu = 2W \tan\alpha/\lambda$, and is illustrated in figure 16(*b*) for the choice $\lambda = 1$. Note that the lift force predicted by (4.6), (4.9) and (4.10) is not sufficient to support the paddle when the moment becomes sufficiently large. Instead the paddle rests on the bottom, and a normal reaction compensates for the unbalanced downward force. The wetted length and $h_T = 0$ then become independent of moment, as seen for the example with the larger angle of attack in figure 16(*b*). The qualitative behaviour of the theoretical curves in figure 16(*b*) is similar to the experimental data of figure 7.

An alternative prescription of Q_L is suggested by Tuck & Dixon (1989) for flow beneath a surfboard; they use the model of Green (1935), which includes the ejected splash jet, and suggest that all the flow into the jet is diverted around the sides of the surfboard. Thus Q_L is taken to be the water flux into the jet (calculated as in the next section), and in this case the resulting force (4.6) turns out to be proportional to d, exactly as in (3.4). We prefer the current formulation in view of the absence of a jet in the experiments, although the results for l and h_T are not qualitatively different between the two versions of the model.

5. A model for the skipping states

As alluded to earlier, and shown schematically in figure 17, our explanation for the destabilisation of the planing state and the persistence of skipping is the build-up of the wedge of fluid ahead of the paddle so that it leaves the water higher than where it entered. The area over which the water pressure acts is therefore not simply a function of depth beneath the undisturbed water level but varies in a more complicated way throughout the course of the collision. This fact was realised by Wagner (1932) in his early work studying impact forces on sea plane floats. He noticed that the water around the impacting float rises up to meet it so that the wetted area expands rapidly outwards from the contact point; the region over which the water pressure is appreciable is not simply the region beneath the undisturbed water surface, but a larger region.

A sizeable literature has been built up extending these ideas, and the so-called Wagner problem involves determining the short-time behaviour of the wetted region, and the resulting force, on a vertically impacting object (Howison *et al.* 1991; Howison, Ockendon & Oliver 2002; Korobkin & Iafrati 2005). A key feature that emerges is the prediction of the splash jet from the edge of the wetted region. This is very evident also during the skipping motion in our experiments, as is seen in figure 8. The theory predicts that the pressure within the jet itself contributes only a small fraction of the force on the object; the dominant force is provided by the pressure *within* the wetted region.
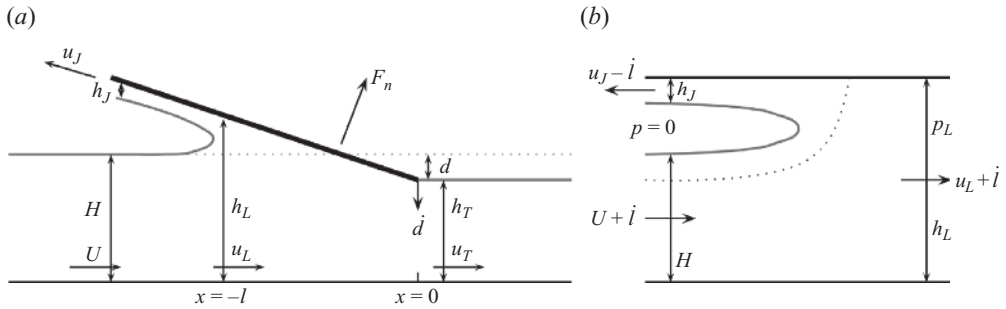
(*a*)

(*b*)

FIGURE 18. (*a*) Geometry of the shallow-water skipping model, with a jet of thickness h_J ejected ahead of the paddle and a stagnation point on the paddle at $x = -l$. (*b*) Geometry of the leading-edge region, in the frame in which it is stationary (moving at speed $\dot{l}$ relative to (*a*)).

5.1. *Shallow-water skipping model*

Accounting for the full details of the flow around the paddle is complicated, and instead we again opt to capture some of the main ideas in a simpler description based on another shallow-water set-up. For the skipping state, however, it is necessary to include the ejected jet, and the new geometry is shown in figure 18. The situation is similar to the model of Tuck & Dixon (1989), which we generalise below for the unsteady case. Once again, the shallow setting limits the theory to small angles of attack, unlike the experiments. Nevertheless, it is our intention to understand why the paddle should be unstable to a skipping state at all, and we do not attempt to reproduce the entire range of experimental results.

In the model, the water ejected into the jet is assumed to disappear; we do not calculate its trajectory as it moves up and separates from the paddle and falls back into the stream under gravity. This is justified on the basis of the experiments in which, during skipping, the jet remains attached to the paddle for longer than the paddle is in contact with the bulk of the stream – it only falls back onto the stream once the paddle has become airborne again, and the splash that is then created is quickly washed downstream. Thus, once the water is diverted into the jet it plays no continuing role in the bounce dynamics.

For the geometry shown in figure 18, the depths h and h_L are defined as in (4.1) and (4.2) but now depend on time via $d(t)$ and $l(t)$. We take $x = -l(t)$ to be the instantaneous position of the stagnation point; the theory described here will make use of the small aspect ratio (*s*) to reduce the dynamics of the 'turnover region' near the stagnation point to a set of jump conditions.

5.2. *Beneath the paddle*

The flow under the paddle satisfies the shallow-water equations:

$$h_t + (hu)_x = 0, \tag{5.1}$$

$$\rho(u_t + uu_x) + p_x = 0. \tag{5.2}$$

At the trailing edge $x = 0$, $h = h_T(t) = H - d(t)$ is determined by the displacement of the paddle, and the pressure is atmospheric, $p = 0$. At the leading edge $x = -l(t)$, the values $h_L(t)$, $u_L(t)$ and $p_L(t)$ are related to the upstream conditions $h = H$, $u = U$

and $p = 0$, by matching conditions which conserve mass and momentum across the turnover region.

Integrating (5.1) subject to $u = u_L(t)$ at $x = -l(t)$ and (5.2) subject to $p = 0$ at $x = 0$ gives

$$u(x, t) = \left(u_L + \frac{\dot{d}}{s}\right)\frac{h_L}{h} - \frac{\dot{d}}{s}, \tag{5.3}$$

$$\frac{p(x, t)}{\rho} = \frac{1}{2}\left(u_L + \frac{\dot{d}}{s}\right)^2 h_L^2\left(\frac{1}{h_T^2} - \frac{1}{h^2}\right) - \frac{(h - h_T)\ddot{d}}{s^2}$$
$$+ \left[\frac{h_L}{s}\left(\dot{u}_L + \frac{\ddot{d}}{s}\right) + \left(\dot{l} - \frac{\dot{d}}{s}\right)\left(u_L + \frac{\dot{d}}{s}\right)\right]\log\frac{h}{h_T}. \tag{5.4}$$

The normal force on the paddle is therefore given by

$$\frac{F_n(t)}{\rho W} = \int_{-l(t)}^{0}\frac{p(x, t)}{\rho}\,\mathrm{d}x = \frac{1}{2}\frac{h_L - h_T}{s}\left[\frac{(h_L - h_T)h_L}{h_T^2}\left(u_L + \frac{\dot{d}}{s}\right)^2 - \frac{(h_L - h_T)\ddot{d}}{s^2}\right]$$
$$+ \left[\frac{h_L}{s}\left(\dot{u}_L + \frac{\ddot{d}}{s}\right) + \left(\dot{l} - \frac{\dot{d}}{s}\right)\left(u_L + \frac{\dot{d}}{s}\right)\right]\left(\frac{h_L}{s}\log\frac{h_L}{h_T} - \frac{h_L - h_T}{s}\right). \tag{5.5}$$

This can be used in the equation of motion for the paddle (3.3) to determine $d(t)$; however since h_L and h_T are given in terms of d and l by (3.2) and (4.2), we require two more equations for $l(t)$ and $u_L(t)$ in order to do this.

5.3. *At the leading edge*

The turnover region at the leading edge is small, which means the dynamics within this region can be considered to be in a steady state once we move into a frame in which the stagnation point is stationary. This can be shown using a formal expansion in the small aspect ratio s, and figure 18(b) shows the approximate geometry in this region; note that the assumption that s is small means that the paddle is approximately horizontal on this scale, at height $h_L(t)$. The incoming stream has height H, and the ejected jet has thickness $h_J(t)$. The pressure on the left vanishes (atmospheric), whilst that on the right matches with $p_L = p(-l(t), t)$ in (5.4).

Tuck & Dixon (1989) showed how to solve for the full details of the steady flow in figure 18(b) using complex variable methods; for our purposes this is unnecessary, and it is sufficient to call upon global conservation of mass and momentum across the region:

$$H(U + \dot{l}) = h_L(u_L + \dot{l}) + h_J(u_J - \dot{l}), \tag{5.6}$$
$$\rho H(U + \dot{l})^2 - h_L p_L = \rho h_L(u_L + \dot{l})^2 - \rho h_J(u_J - \dot{l})^2. \tag{5.7}$$

We also make use of Bernoulli's principle on the streamlines along the bottom and free surface, implying

$$U + \dot{l} = u_J - \dot{l}, \tag{5.8}$$
$$p_L + \tfrac{1}{2}\rho(u_L + \dot{l})^2 = \tfrac{1}{2}\rho(U + \dot{l})^2. \tag{5.9}$$

Combining (5.6)–(5.9) we find

$$u_J = U + 2\dot{l}, \tag{5.10}$$

$$u_L = U - 2(U + \dot{l})\left(1 - \frac{H^{1/2}}{h_L^{1/2}}\right), \tag{5.11}$$

$$h_J^{1/2} = h_L^{1/2} - H^{1/2}, \tag{5.12}$$

$$p_L = 2\rho(U + \dot{l})^2 \frac{H^{1/2}}{h_L^{1/2}} \left(1 - \frac{H^{1/2}}{h_L^{1/2}}\right). \tag{5.13}$$

Equation (5.11) provides the required expression for $u_L(t)$, and equating p_L in (5.13) with $p(-l(t), t)$ in (5.4) provides the final closure condition to determine $l(t)$.

5.4. Full equations

The complete model reduces to a set of three coupled ordinary differential equations for d, l and u_L, following from (3.3) and (5.11) and equating (5.4) and (5.13):

$$
\begin{aligned}
I\ddot{d} = M - \rho W a \cos(\alpha - \beta) &\left\{ \frac{1}{2} \frac{h_L - h_T}{s} \left[\frac{(h_L - h_T)h_L}{h_T^2} \left(u_L + \frac{d}{s} \right)^2 - \frac{\ddot{d}(h_L - h_T)}{s^2} \right] \right. \\
&+ \left[\frac{h_L}{s} \left(\dot{u}_L + \frac{\ddot{d}}{s} \right) + \left(\dot{l} - \frac{\dot{d}}{s} \right) \left(u_L + \frac{\dot{d}}{s} \right) \right] \\
&\left. \times \left(\frac{h_L}{s} \log \frac{h_L}{h_T} - \frac{h_L - h_T}{s} \right) \right\} - \nu \dot{d},
\end{aligned}
\tag{5.14}
$$

$$u_L = U - 2(U + \dot{l})\left(1 - \frac{H^{1/2}}{h_L^{1/2}}\right), \tag{5.15}$$

$$
\begin{aligned}
\frac{1}{2}\left(u_L + \frac{\dot{d}}{s} \right)^2 \left(\frac{h_L^2}{h_T^2} - 1 \right) - \frac{(h_L - h_T)\ddot{d}}{s^2} &+ \left[\frac{h_L}{s} \left(\dot{u}_L + \frac{\ddot{d}}{s} \right) \right. \\
\left. + \left(\dot{l} - \frac{\dot{d}}{s} \right) \left(u_L + \frac{\dot{d}}{s} \right) \right] \log \frac{h_L}{h_T} &= 2(U + \dot{l})^2 \frac{H^{1/2}}{h_L^{1/2}} \left(1 - \frac{H^{1/2}}{h_L^{1/2}} \right),
\end{aligned}
\tag{5.16}
$$

where

$$h_T = H - d, \qquad h_L = H - d + sl. \tag{5.17}$$

These equations hold only when the paddle is in the water; when it is out of the water, the equation of motion is simply

$$I\ddot{d} = M - \nu \dot{d}. \tag{5.18}$$

The switch between (5.18) and (5.14)–(5.17) occurs when the paddle enters the water and d switches sign from negative to positive (at which time $l = 0$ and $u_L = U$). The switch back to (5.18) occurs when the paddle leaves the water, which occurs when l first reaches 0 (and arises when d has already become negative again).

The equations are straightforward to solve numerically, and solutions are shown in figures 19 and 20. The system in (5.14)–(5.17) has regular singular points at the moment of entry, when d and l are zero, so a small-time series expansion is used to build a solution each time the paddle enters the water. The initial conditions and parameters used in figure 19 are the same as for the solution of (3.6) shown in figure 15, but the predicted behaviour is very different. The paddle bounces to increasingly higher amplitudes and quickly settles into a constant-amplitude skipping state. This saturation is due to the water ejected in the jet – as the amplitude of bounces increases, more and more water is lost to the jet, and this provides a limiting dissipative mechanism.
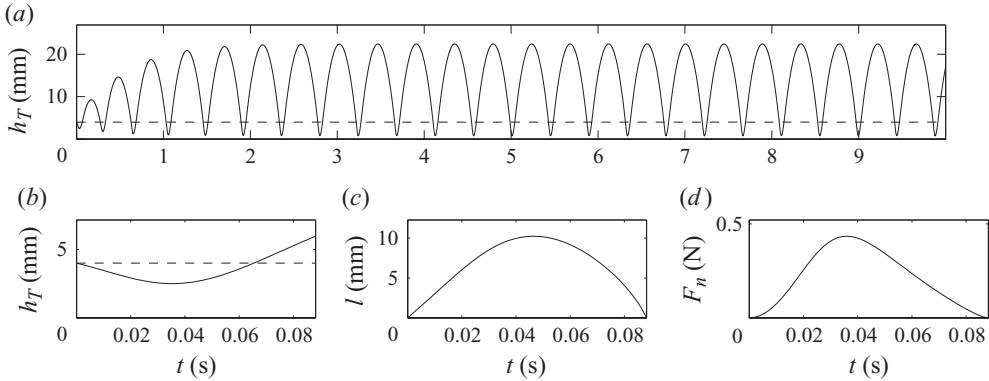
FIGURE 19. (*a*) Trajectory of paddle according to the shallow-water model (5.14)–(5.18). (*b*) The paddle tip position, (*c*) the wetted length and (*d*) the normal force, during the first bounce. The parameters are $H = 4$ mm, $U = 1.1$ m s^{-1}, $\alpha = 30°$, $M = 0.03$ N m, $I = 0.03$ kg m, $\beta = 20°$, $a = 0.35$ m and $\nu = 0$, and the initial vertical entry velocity is 50 mm s^{-1} (i.e. $d = 0$, $\dot{d} = 50$ mm s^{-1} at $t = 0$), as in figure 15.
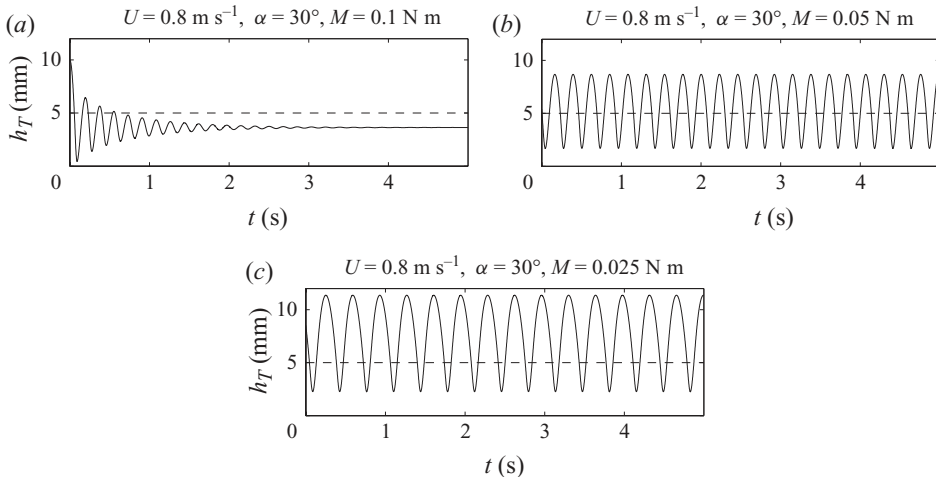

FIGURE 20. Sample trajectories predicted by the shallow-water skipping model (5.14)–(5.18) for different moments M: (*a*) 0.1, (*b*) 0.05 and (*c*) 0.025 N m. In (*a*) the paddle is released from 10 mm above the water ($d = -10$ mm, $\dot{d} = 0$ at $t = 0$), whilst (*b*) and (*c*) show periodic oscillations. The other parameters are $U = 0.8$ m s^{-1}, $H = 5$ mm, $\alpha = 30°$, $I = 0.03$ kg m, $a = 0.35$ m, $\beta = 20°$, $W = 96$ mm and $\nu = 0.09$ kg m s^{-1}.

Notice that the solution for each individual bounce predicts that the paddle is above the undisturbed water level for a significant part of the collision, just as is suggested by the data in figure 8. The maximum of the wetted length occurs after the maximum depth of the paddle, and the force is asymmetrical, increasing quadratically with the depth of the paddle on entry, rather than linearly as would be predicted by (3.5).

Sample trajectories produced by the model are shown in figure 20 and can be compared with those from the experiment shown in figure 3. The general pattern of skipping motion (see figure 21) is the same as that found in the experiments; larger-amplitude, lower-frequency skipping occurs at lower moments, and as the moment is increased the amount of time spent in the water increases.
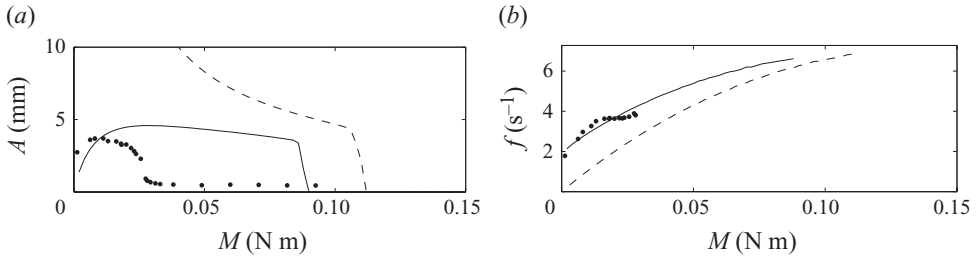
FIGURE 21. Bifurcation diagram showing the (a) amplitude and (b) frequency of skipping oscillations predicted by the shallow-water model (5.14)–(5.18), together with some experimental data shown by the dots. The solid line shows the theory with a crude estimate for the damping of $\nu = 0.2 \,\text{kg}\,\text{m}\,\text{s}^{-1}$, and the dashed line shows the case with no damping $\nu = 0$. The other parameters are $\alpha = 24°$, $I = 0.03 \,\text{kg}\,\text{m}$, $a = 0.35 \,\text{m}$, $\beta = 20°$, $W = 96 \,\text{mm}$, $U = 0.88 \,\text{m}\,\text{s}^{-1}$ and $H = 4 \,\text{mm}$.

For large enough moments the regular skipping state ceases to exist, and any initial oscillations decay to the steady surfing solution of Tuck & Dixon (1989), in which

$$l = 2d^{1/2}(H^{1/2} + d^{1/2})\cot\alpha, \qquad F_n = 2\rho W U^2 d \cot\alpha, \qquad (5.19)$$

and therefore

$$d = \frac{M\tan\alpha}{2a\rho W U^2 \cos(\alpha - \beta)}. \qquad (5.20)$$

Notice that this steady force is the same (for small α) as in (3.4); it varies linearly with the entry depth d, as is also approximately the case in (3.5) (although the multiplying constant there is slightly different). As discussed in the previous section, this steady state is hard to relate to the observed planing states because the jet collapses into the turbulent wedge. Nevertheless, in this model the onset of skipping corresponds to a loss of stability of this steady state, which we therefore study below.

5.5. Instability

A linear stability analysis of (5.14)–(5.17) shows that the steady state (5.20) is unstable for moments M less than a critical moment M_c, which depends upon the parameters α and U. The predicted region of instability is shown in figures 22(a)–22(c), and bifurcation diagrams for varying moment are shown in figure 21. The qualitative picture is in many ways similar to what was observed in the experiments. In particular, the threshold moment for instability increases with the velocity and decreases for large paddle angles, as appears to be the case in figure 4. The predicted amplitudes of skipping are also similar to the observed data included in the figure.

If we ignore the friction term, the threshold for skipping can be conveniently described using the two dimensionless parameters

$$\Gamma = \frac{\tan\alpha}{a\cos(\alpha - \beta)\rho W H}\frac{M}{U^2}, \qquad \Delta = \frac{\tan^2\alpha \,\mathscr{I}}{a^2\cos\beta\cos(\alpha - \beta)\rho W H^2}, \qquad (5.21)$$

as shown in figure 22(d). For fixed α, it follows immediately that the threshold moment should scale with U^2 as seen in figure 22(a) and as also appears to be the case for the experimental data in figure 10.

The bifurcation in this skipping model disagrees with the experimental findings in two noticeable respects: the predicted critical moment is somewhat larger than was found in the experiments, and the bifurcation is always supercritical, with no evidence
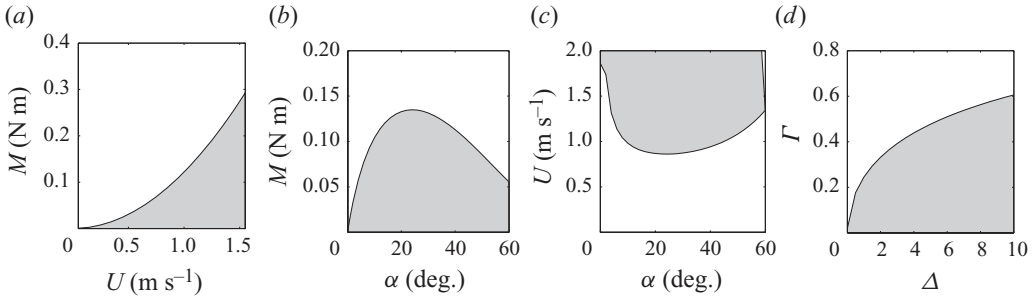
FIGURE 22. Linear instability region of the steady surfing state of (5.14)–(5.18) with no friction $\nu = 0$, with (*a*) fixed angle of attack $\alpha = 36°$ and varying moment M and velocity U; (*b*) varying angle of attack and moment, with fixed velocity $U = 1\,\mathrm{m\,s^{-1}}$; and (*c*) varying angle of attack and velocity, with fixed moment $M = 0.1\,\mathrm{N\,m}$. (*d*) The instability region in terms of the two dimensionless parameters (5.21).

of an intermediate bistable regime. These discrepancies are most likely due to the unphysical nature of this model's steady state, in that it involves the splash jet being constantly ejected ahead of the paddle. The recirculating water could be accounted for in the model by assuming that the jet falls back onto the incoming stream and that the water in it simply adds to the stream's depth, by the amount h_J given by (5.12), without changing its speed. Replacing the incoming depth H in the model by $H + h_J$, a little algebra recovers the steady planing state of §4 with $h_T = H$ (i.e. $d = 0$), and F_n given in terms of l by (4.6). Thus the two models are not entirely inconsistent. However, to predict correctly the unstable transition from planing to skipping would require including gravity fully in the unsteady skipping model (5.14)–(5.18).

6. Conclusions

We have performed a series of experiments studying the dynamics of an inclined paddle suspended above a shallow stream and have found distinct regimes of steady planing, continual skipping and sloshing. When the paddle is following ballistic trajectories interrupted by bounces on the water surface, the system is equivalent to that of a skimming stone constrained to move with constant horizontal velocity.

The planing state involves a turbulent foaming wedge of water built up ahead of the paddle, and the size of this wedge increases as the moment (effective weight) of the paddle is increased. The properties of the steady states can be understood using the simple shallow-water description in §4, provided that one accounts for any flow that may be diverted around the sides of the paddle.

When the moment is reduced sufficiently, or the stream velocity is increased, there is a bifurcation from the planing state to a regular skipping state, with a well-defined amplitude and frequency. For large angles of attack, this bifurcation is subcritical, and there is sometimes a large bistable region of parameter space in which the paddle can either skip continuously or plane at a steady depth. A second shallow-water model, in which we allow for a jet to be ejected from the splash-up region ahead of the paddle, was proposed to explain the skipping state. Importantly, the wetted length of the paddle is not simply a function of the paddle position but varies in a more complicated way throughout the course of the collision time. This can be thought of as a nonlinear deformation of the surface that converts horizontal kinetic energy of the water into vertical motion of the paddle, resulting in a *superelastic* bounce.

However, the model gives only qualitative agreement with the experiments, and the quantitative comparison is poor. Partly, this is because the major assumption of the model, that the angle of attack is small, is not true for our experiments. The experiments were not performed for very low angles of attack to afford a better comparison with the theory because of some geometrical limitations of the experimental set-up, and even at the lowest angle used (24°) there are significant discrepancies. An improved model for large angles of attack is even more difficult to formulate in view of the complicated geometry of the flow in the jet. We nevertheless have found that the results of the shallow-water model are qualitatively comparable to what is observed experimentally and therefore have some confidence that the underlying physics is similar.

A further theoretical issue is that our two models, one of the planing state and one for the skipping state, do not overlap. In the planing state the water that moves up the paddle recirculates in a turbulent wedge upstream. In the skipping model the water is thrown up into the jet and re-enters the water surface only after the paddle has bounced. A model that can contain these two cases and thus smoothly model the increasing amplitude of oscillations from the planing state is substantially more difficult to construct.

We suggest that future experimental work might concentrate on a more careful and detailed exploration of parameter space; in particular it would be interesting to look at shallower angles of attack, to see if there is a more systematic dependence on this parameter than was uncovered here. It would also be worthwhile to investigate different paddle shapes: circular disks more like a skipping stone, triangular wedges similar to a speed boat's hull and barrel shapes like the bouncing bomb. Is continual skipping also possible for such shapes? And are certain shapes more unstable than others?

One might also wonder how much the results are affected by the shallowness of the stream and whether the same behaviour would be found on a much deeper flow. Preliminary experiments were in fact carried out on deeper water, by suspending the paddle above a large rotating tank (Hewitt 2008). Similar continual skipping behaviour was found then, but the set-up was abandoned because of difficulties eliminating the wake of previous bounces. In any event, our explanation for why skipping can continue indefinitely surrounds the rise of water ahead of the entering paddle. The shallowness of the stream is therefore not fundamental; even though in deep water the splash-up region will tend to be smaller than in shallow water, it is still there, and we therefore expect the same instability to allow continual skipping.

For the wide paddle, when the applied moment was sufficient to dam an extensive pool of water upstream, the steady planing state was also unstable to sloshing modes, resulting from a resonance between oscillations of the paddle and seiche modes in that reservoir. This phenomenon can be studied in the much simpler geometry of a flat tank (Scolan 2009); a separate paper provides a much fuller discussion (Hewitt, Scolan & Balmforth 2010) and draws an analogy with the mechanism generating musical sounds in woodwind instruments like the clarinet.

REFERENCES

BOCQUET, L. 2003 The physics of stone skipping. *Am. J. Phys.* **71**, 150–155.

CLANET, C., HERSEN, F. & BOCQUET, L. 2004 Secrets of succesful stone-skipping. *Nature* **427**, 29.

GREEN, A. E. 1935 The gliding of a plate on a stream of finite depth. *Proc. Camb. Phil. Soc.* **31**, 589–603.

GREEN, A. E. 1936 The gliding of a plate on the surface of a stream. *Proc. Camb. Phil. Soc.* **32**, 248–252.

HEWITT, I. J. 2008 Continual skipping on water. *Rep. 50th GFD Summer School*. Woods Hole Oceanographic Institute.

HEWITT, I. J., SCOLAN, H. & BALMFORTH, N. J. 2010 Flow destabilized seiches in a reservoir with a movable dam; the water clarinet. *J. Fluid Mech.* (submitted).

HOWISON, S. D., OCKENDON, J. R. & OLIVER, J. M. 2002 Deep- and shallow-water slamming at small and zero deadrise angles. *J. Engng Maths* **42**, 373–388.

HOWISON, S. D., OCKENDON, J. R. & OLIVER, J. M. 2004 Oblique slamming, planing and skimming *J. Engng Maths* **48**, 321–337.

HOWISON, S. D., OCKENDON, J. R. & WILSON, S. K. 1991 Incompressible water-entry problems at small deadrise angles. *J. Fluid Mech.* **222**, 215–230.

JOHNSON, W. 1998 The ricochet of spinning and non-spinning spherical projectiles, mainly from water. Part II. An outline of theory and warlike applications. *Intl J. Impact Engng* **21**, 25–34.

VON KÁRMÁN, T. 1929 The impact of sea planes during landing. *NACA Tech. Note* 321.

KOROBKIN, A. 1999 Shallow-water impact problems. *J. Engng Maths* **35**, 233–250.

KOROBKIN, A. & IAFRATI, A. 2005 Hydrodynamic loads during initial stage of floating body impact *J. Fluids Struct.* **21**, 413–427.

MAYO, W. L. 1945 Analysis and modification of theory for impact of seaplanes on water. *NACA Rep.* 810.

PAYNE, P. R. 1994 The water rise in front of a model planing hull. *Exp. Fluids* **17**, 96–104.

ROSELLINI, L., HERSEN, F., CLANET, C. & BOCQUET, L. 2005 Skipping stones. *J. Fluid Mech.* **543**, 137–146.

SCOLAN, H. 2009 Flow-destabilized modes with a movable dam. *Rep. 51st GFD Summer School*. Woods Hole Oceanographic Institute.

SUGIMOTO, T. 2003 Mechanics of the surf skimmer revisited. *Am. J. Phys.* **71**, 144–149.

TING, L. & KELLER, J. B. 1974 Planing of a flat plate at high Froude number. *Phys. Fluids.* **17**, 1080–1086.

TUCK, E. O. & DIXON, A. 1989 Surf-skimmer planing hydrodynamics. *J. Fluid Mech.* **205**, 581–592.

WAGNER, H. 1932 Über Stoß-und gleitvorgänge an der Oberflaäche von Flüssigkeiten [Phenomena associated with impacts and sliding on liquid surfaces]. *Z. Angew. Math. Mech.* **12**, 193–215.